Editors' Suggestion

Observation of Drastic Electronic-Structure Change in a One-Dimensional Moiré Superlattice

Sihan Zhao,[1,*] Pilkyung Moon,[2,3] Yuhei Miyauchi,[4] Taishi Nishihara,[4] Kazunari Matsuda,[4] Mikito Koshino,[5] and Ryo Kitaura[6,†]

[1]*Department of Physics, University of California at Berkeley, Berkeley, California 94720, USA*
[2]*Arts and Sciences, NYU Shanghai, Shanghai 200122, China and NYU-ECNU Institute of Physics at NYU Shanghai, Shanghai 200062, China*
[3]*State Key Laboratory of Precision Spectroscopy, East China Normal University, Shanghai 200062, China*
[4]*Institute of Advanced Energy, Kyoto University, Uji, Kyoto 611-0011, Japan*
[5]*Department of Physics, Osaka University, Toyonaka 560-0043, Japan*
[6]*Department of Chemistry, Nagoya University, Nagoya 464-8602, Japan*

(Received 3 July 2019; revised manuscript received 25 November 2019; accepted 16 January 2020; published 9 March 2020)

We report the first experimental observation of a strong-coupling effect in a one-dimensional moiré superlattice. We study one-dimensional double-wall carbon nanotubes (DWCNTs) in which van der Waals–coupled two single nanotubes form a one-dimensional moiré superlattice. We experimentally combine Rayleigh scattering spectroscopy and electron beam diffraction on the same individual DWCNTs to probe the optical transitions of the structure-identified DWCNTs in the visible spectral range. Among more than 30 structure-identified DWCNTs examined, we experimentally observed and identified a drastic change of the optical transition spectrum in a DWCNT with chirality (12,11)@(17,16). The origin of the marked change is attributed to the strong intertube coupling effect in the moiré superlattice formed by two nearly armchair nanotubes. Our numerical simulation is consistent with the experimental findings.

DOI: 10.1103/PhysRevLett.124.106101

Engineering electronic band structures through the formation of a moiré superlattice has enabled the discoveries of exotic physics in two-dimensional (2D) van der Waals–coupled heterostructures [1–16]. Such band structure engineering through the formation of a moiré superlattice can lead to the significant alteration of the electronic properties in the coupled heterostructures. One of the impressive examples is to control the mutual angle between two graphene monolayers to form twisted bilayer graphene [5–9]. The flat band caused by a moiré superlattice structure gives rise to a Mott insulating state and a superconducting state at certain "magic" angles, which, on the other hand, do not exist in the pristine monolayers. A moiré superlattice formed between 2D semiconductors also leads to the observation of moiré excitons which is a direct consequence of the drastic band structure change caused by a moiré superlattice [11–16].

While there has been rapid progress on understanding the moiré physics in 2D van der Waals heterostructures, experimental studies on moiré superlattices in one-dimensional (1D) systems are still limited, and no clear evidence on strong electronic-structure modification has been found and explained in structure-identified 1D moiré superlattices [17–20]. Double-wall carbon nanotubes (DWCNTs), which correspond to a "rolled-up" version of twisted bilayer graphene, naturally provide an ideal platform to experimentally probe the moiré physics in 1D. Theoretically, it was assumed that the electronic band structures of realistic DWCNTs are close to those of the individual constituent two single nanotubes, and the effect of the intertube coupling is perturbative [21–24]. Most previous experimental observations on the intertube coupling effect are well explained within the weakly perturbative regime [25–28]. However, a recent theoretical study predicted that there are special cases where the moiré superlattice potential causes strong coupling between two single nanotubes and can result in completely different band structures [29].

Here we show the experimental evidence of the strong-coupling effect in 1D moiré superlattices where the moiré superlattice potential significantly alters the electronic band structures in DWCNTs. The lattice structure of each constituent nanotube, and, consequently, the moiré superlattice formed in the DWCNT, is determined by electron beam diffraction, and the corresponding electronic transitions of the same DWCNT are probed by Rayleigh scattering spectroscopy in the visible spectral range. Though rarely observed in all examined DWCNTs, one specific DWCNT shows a drastic change in its Rayleigh scattering spectrum, which is assigned to be a direct consequence of the strong coupling between two constituent single nanotubes. The calculated band structure and optical absorption spectra with intertube coupling within the effective continuum model support our experimental

interpretation. Our experimental observation of a strong-coupling effect in 1D DWCNT moiré superlattices can open up new opportunities to explore the rich moiré physics in 1D systems.

To investigate the intrinsic moiré physics in DWCNTs, we directly grew suspended DWCNTs with high quality across an open slit (~30 μm in width) by chemical vapor deposition. We studied the individual DWCNTs that are isolated from other nanotubes. The structure (i.e., the chirality) of each constituent single nanotube comprising a DWCNT was determined by nanobeam electron diffraction with a transmission electron microscope operated at 80 keV (JEOL-2100F). Electronic transitions of the DWCNTs with known chiralities were probed by Rayleigh scattering spectroscopy. In brief, a broadband light from a supercontinuum laser source (1.2–2.75 eV) was focused on the central part of the suspended DWCNT samples, and the laser light was polarized along the nanotube axis to probe optical transitions within the same 1D subbands. The light scattered by the nanotube was collected and directed to a CCD camera and a spectrometer. The Rayleigh scattering spectra were obtained by normalizing the measured scattered light intensity with incident laser intensity.

Most of the structure-identified DWCNTs were found in a weak-coupling regime [26,28]. Two representative Rayleigh spectra for individual DWCNTs with weak coupling are shown in Figs. 1(a) and 1(b). The chiralities of the two DWCNTs are determined as (15,13)@(21,17) and (23,4)@(22,18) by nanobeam electron diffraction, respectively. (15,13) and (21,17) in (15,13)@(21,17) correspond to the chirality of the inner nanotube and outer nanotube, respectively, and we keep this notation for indexing DWCNTs throughout the Letter. As clearly seen in the spectra, multiple pronounced optical resonances are observed in both DWCNTs. Each optical resonance in the spectra arises from the dipole-allowed interband transitions within the same 1D subbands from inner and/or outer nanotubes. For example, in (15,13)@(21,17) shown in Fig. 1(a), four peaks indicated by the blue arrows are assigned to the S_{33}, S_{44}, S_{55}, and S_{66} optical transitions from the outer nanotube (21,17), and those indicated by the red arrows are the S_{33} and S_{44} optical transitions from the inner nanotube (15,13).

To investigate intertube interaction in detail, we precisely determine the resonant transition energies through peak deconvolution with fitting each of the resonances by the form of $I(\omega) \propto \omega^3|\chi(\omega)|^2$, where $\chi(\omega) \sim A_0 + [(\omega_0 - \omega) - i\gamma/2]^{-1}$. $I(\omega)$, $\chi(\omega)$, γ, and A_0 represent the peak intensity, optical susceptibility, full width at half maximum (FWHM) associated with a resonance peaked at ω_0, and nonresonant constant background that accounts for the asymmetric Rayleigh peak shape [30], respectively. The fitted curve of each "Lorentzian-like" optical resonance is shown as the black line, and the overall fitted spectrum is presented by the green line. The optical transition energies (i.e., ω_0) for the two DWCNTs are summarized in Supplemental Material, Sec. I [31]. Comparing with the transition energies in isolated single nanotubes in air [32], all the optical resonances observed in DWCNTs with weak coupling exhibit noticeable energy redshifts (some can show blueshifts) by a few tens to 200 meV.

While most of the DWCNTs investigated are within the weak-coupling regime, where DWCNTs show almost identical electronic transitions to those of each individual constituent nanotube, we experimentally identified two DWCNTs whose electronic transitions are theoretically predicted to be very different from those of constituent single nanotubes due to a nonperturbative intertube coupling between the inner and outer nanotubes [29]. Theoretically, van der Waals coupling between the inner and outer nanotubes in DWCNT moiré superlattices is

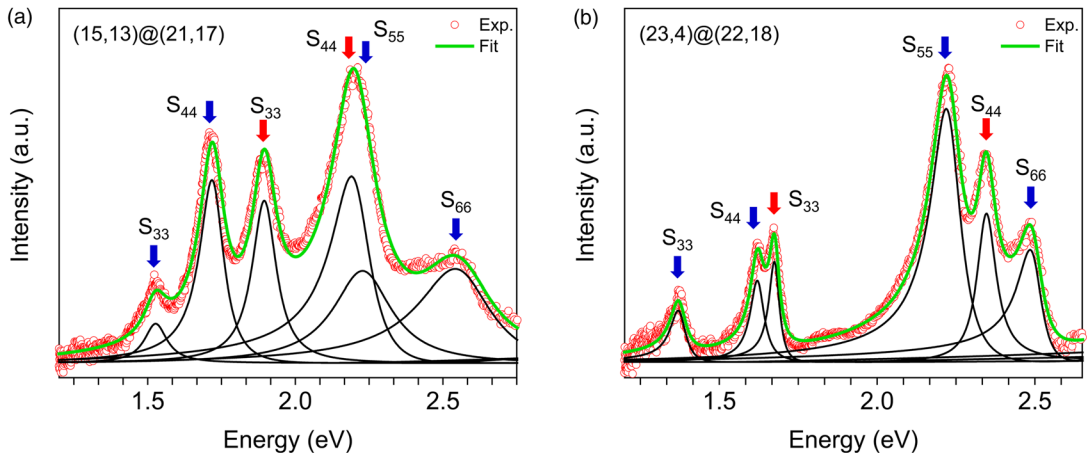

FIG. 1. Rayleigh scattering spectra of two typical structure-identified DWCNTs with weak coupling. (a) Spectrum for DWCNT (15,13)@(21,17). (b) Spectrum for DWCNT (22,4)@(23,18). In both (a) and (b), red and blue arrows mark the optical transitions for inner and outer nanotubes, respectively. The experimental data are presented by red open circles. Each fitted optical transition is presented with a black curve, and the overall fitted spectrum is shown by a solid green line.

essentially characterized by the relative orientation of the chiral vectors (chiralities) of the inner and outer nanotubes, C and C'. Significant modification of the band structure takes place under two different conditions, which we call the strong-coupling case and the flatband case. The former occurs when C and C' are nearly parallel to each other and, at the same time, the difference of two chiral vectors $C' - C$ is parallel to the armchair direction. Then the moiré superlattice potential makes the resonant coupling between the states of constituent nanotubes, and this leads to a drastic energy shift of the subband edges. The latter case occurs under the condition that C and C' are nearly parallel and $C' - C$ is parallel to the zigzag direction. There, a long period moiré interference potential turns the original single nanotube bands into a series of nearly flat bands. When C and C' meet either of these two conditions, the electronic structures of DWCNTs become drastically different from the simple sum of constituent single nanotubes [29].

It is easy to see that neither of the two weak-coupled DWCNTs shown in Fig. 1 meets the conditions described above. In fact, there is lot less chance to have a DWCNT meeting the two criteria. For example, the probability for DWCNTs to satisfy the former criterion is only ~0.6% (Supplemental Material, Sec. II [31]). Although we still expect some moderate change of electronic structures in DWCNTs near the criteria, the effects of coupling become weaker as the configuration of C and C' deviates from the criteria. Hereafter, we will focus on a strong-coupling case, the (12,11)@(17.16) DWCNT, which accurately matches the former criterion. Experimental data for the (14,3)@(23,3) DWCNT which approximately matches the latter condition are shown in Supplemental Material, Secs. III and IV [31].

Figure 2(a) displays a transmission electron microscopy (TEM) image of a DWCNT in the strong-coupling regime. Although the TEM image becomes blurred away from the slit edge due to the vibration arising from the suspended structure, it is clear that there are contrasts originating from both inner and outer nanotubes. Judging from the TEM image, this DWCNT comprises an outer nanotube with a diameter of ~2.2 nm and an inner nanotube with a diameter of ~1.5 nm with a reasonable intertube distance (~0.35 nm). To unambiguously determine the physical structure of each nanotube, electron beam diffraction is employed, and an observed diffraction pattern is presented in Fig. 2(b). Similar to single chiral nanotubes in general, the diffraction pattern of a DWCNT shows sets of mutually twisted hexagonal patterns, which arise from a hexagonal lattice of graphitic layers. Prior to any analysis in detail [37], Fig. 2(b) shows that the two constituent nanotubes are both nearly armchair nanotubes. The equatorial line in the DWCNT diffraction pattern exhibits a "beatinglike" oscillation in intensity, which is absent in diffraction patterns in single nanotubes. This unique intensity oscillation originates from the interference of electron waves scattered by

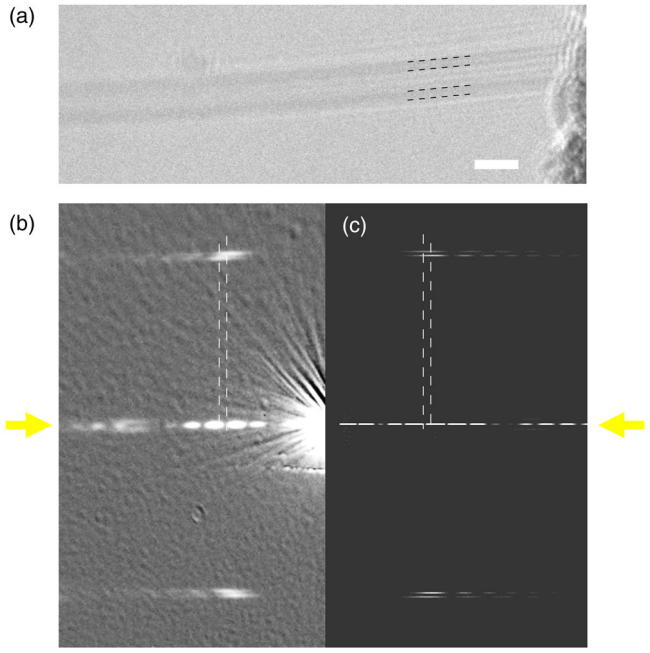

FIG. 2. Structure characterization of a DWCNT (12,11)@(17,16) showing a strong-coupling effect. (a) TEM image of the DWCNT. Dashed lines indicate the walls of two constituent nanotubes. The scale bar is ~2 nm. (b) Experimental electron diffraction pattern. (c) Simulated electron diffraction pattern of a DWCNT with chirality (12,11)@(17,16). Two yellow arrows indicate the position of the equatorial line in the diffraction pattern. The dashed lines are eye guidance to show one of the key identities between the experiment and simulation.

two nanotubes in the radial direction in a DWCNT. Because of the high sensitivity of the interference to diameter and/or chirality of each nanotube, the oscillation profile along the equatorial line serves as a decisive feature for unambiguous determination of DWCNT chirality. The intensity profile of equatorial line cut in Fig. 2(b) is further shown in Supplemental Material, Sec. V [31]. Based on the analysis procedures reported in the literature [38], the chirality for the inner nanotube is determined to be (12,11), and that for the outer nanotube is (17,16). The simulated diffraction pattern of DWCNT (12,11)@(17,16) is shown in Fig. 2(c) for comparison, which shows an excellent agreement with the observed diffraction pattern in the experiment. We note that one of the key identities between Figs. 2(b) and 2(c) is indicated by dashed lines, where the relative position for features on and outside the equatorial line sensitively depends on the detailed chirality of each constituent single nanotube. We show in Supplemental Material, Sec. VI [31], the simulated pattern of a DWCNT with chirality (12,11)@(16,15), where the chirality of the outer nanotube is slightly different from that of the right chirality DWCNT, (12,11)@(17,16). The discrepancy between the experimental result [Fig. 2(b)] and the simulated pattern of (12,11)@(16,15) is apparent. We systematically examine all the possible candidates with simulation and confirme

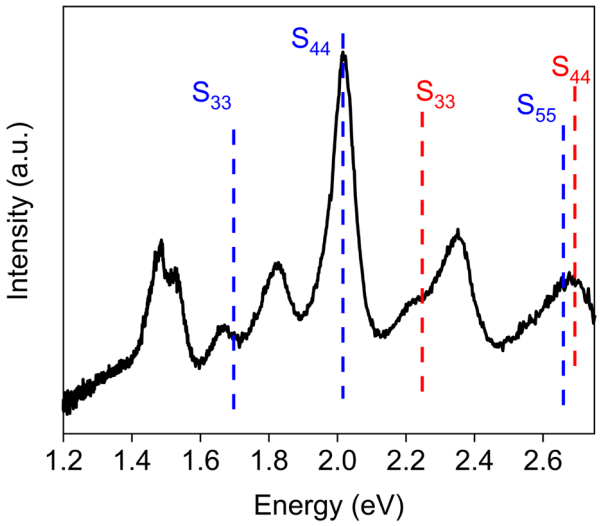

FIG. 3. Rayleigh spectrum of DWCNT (12,11)@(17,16) showing a strong-coupling effect. Experimental data are shown in the solid black line. Dashed red and blue lines indicate the expected optical transition energies for pristine inner and outer nanotubes, respectively.

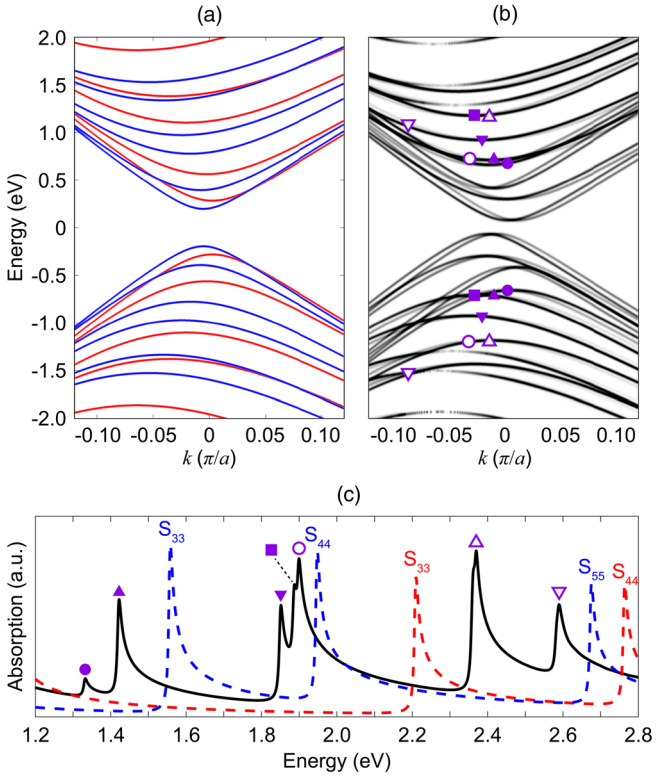

FIG. 4. Theoretical calculation of DWCNT (12,11)@(17,16) within a tight-binding and effective continuum model. (a) Calculated band structure of two pristine nanotubes (12,11) in red and (17,16) in blue in a DWCNT without intertube coupling. (b) Calculated band structure of coupled DWCNT (12,11)@(17,16). (c) Calculated optical absorption spectra for a pristine inner nanotube (dashed red line), a pristine outer nanotube (dashed blue line) and the coupled DWCNT (solid black line). Optical transitions from pristine inner and outer nanotubes are specified (e.g., S_{33}, S_{44}, etc.). Different transitions for the coupled DWCNT in (c) are denoted by different markers which originate from interband transitions as indicated with the same markers in the calculated band structure in (b). Note that the peak at ~2.4 eV (solid black line) is comprised of multiple peaks that are very close in energy. a in the horizontal axises in (a) and (b) denotes the graphene lattice constant.

that only (12,11)@(17,16) matches the experimental result (Supplemental Material, Sec. VII [31]).

The inner and outer nanotubes in (12,11)@(17,16) are nearly armchair nanotubes, which means that C and C' are nearly parallel to each other (~0.4° chiral angle difference). In addition, $C' - C$ is (5,5) that is strictly along the armchair direction. The (12,11)@(17,16) DWCNT is, therefore, a strong-coupled DWCNT, whose band structure can be strongly modified by a 1D moiré superlattice [29]. The Rayleigh spectrum of the same DWCNT (12,11)@(17,16) within the energy range 1.2–2.75 eV is presented in Fig. 3. Identical spectral profiles are obtained at different sample locations (Supplemental Material, Sec. VIII [31]). Markedly, we observe a total of eight well-defined optical resonances over the spectral range 1.2–2.75 eV; the weak peak at ~2.22 eV solely cannot be safely excluded to be a phonon sideband of the strong peak at ~2.02 eV [30,39]. On the other hand, within the same photon energy range, pristine (12,11) has two optical transitions: S_{33} at ~2.23 eV and S_{44} at ~2.68 eV (S_{22} at ~1.18 eV), and pristine (17,16) has three optical transitions: S_{33} at ~1.69 eV, S_{44} at ~2.03 eV, and S_{55} at ~2.66 eV (S_{22} at ~0.90 eV) [32]. These referenced energy positions for inner and outer tubes are indicated by the red and blue dashed lines, respectively, in Fig. 3. Unlike the weak-coupling cases (e.g., Fig. 1), where all optical transitions in DWCNTs correspond to interband transitions of individual constituent nanotubes, (12,11)@(17,16) shows optical resonances that cannot be assigned to those of pristine inner and outer nanotubes. As clearly seen, most of the observed transitions do not match those from each constituent nanotube with showing extra numbers of peaks in contrast to the simple sum of two nanotube spectra. These observations definitely manifest a drastic change of band structure in (12,11)@(17,16).

We attribute the observed drastic change of the optical transition spectrum to the strong-coupling effect arising from the 1D moiré superlattice as the theory predicted [29]. By using the effective continuum model in the framework of a tight-binding (TB) approximation, we calculate the band structure and optical absorption spectrum for (12,11)@(17,16) (see details in Supplemental Material, Sec. IX [31]). The calculated band structure of (12,11)@(17,16) without and with the intertube coupling is shown in Figs. 4(a) and 4(b), respectively. The band structures of pristine inner tube (12,11) and outer tube (17,16) are colored in red and blue in Fig. 4(a), respectively. Figure 4(c) shows the calculated optical absorption

spectrum of the coupled (12,11)@(17,16) (solid black line) as well as the absorption spectra of the pristine inner and outer tubes (dashed red and blue lines, respectively) in the energy range 1.2–2.8 eV. The calculated absorption spectra for the pristine inner and outer nanotubes [dashed red and blue lines, respectively, in Fig. 4(c)] are consistent with experimental data in the literature (dashed lines in Fig. 3) within a precision of ∼100 meV [32] (Supplemental Material, Sec. X [31]).

In contrast to the weak-coupling cases shown in Fig. 1, the strong band hybridization caused by the intertube moiré superlattice potential of (12,11)@(17,16) drastically changes the electronic band structure [Figs. 4(a) and 4(b)] and selection rules of optical absorption from the simple sum of the constituent pristine nanotubes. Overall, our calculated absorption spectrum is qualitatively consistent with the experimental data in the same energy range. Figure 4(c) clearly shows the presence of extra peaks due to moiré superlattice potential as observed in the experiment but not present in the pristine nanotubes. The number of transition peaks in the energy range 1.2–2.8 eV increases from 5 in the pristine nanotubes to 7, which is close to the actually observed number of 8 in Fig. 3. In fact, the peak around 2.4 eV in the theoretical calculation is comprised of multiple peaks that are very close in energy (data not shown), which might be further separated by many-body effects that are not included in our TB calculation. Thus, the theoretical calculation supports the drastic difference between the observed spectrum in Fig. 3 and the spectra of the constituent nanotubes in DWCNT under the strong-coupling condition.

Before ending, we would like to briefly discuss and exclude other possibilities that can potentially lead to the observation of a very distinct spectrum. Structural inhomogeneity such as a change of nanotube chirality, attachment of small nanotubes and/or impurities can cause a very different optical response. In this study, the structure of DWCNT (12,11)@(17,16) is retained the same over the whole suspended region (∼30 μm) which is confirmed by the electron diffraction (Supplemental Material, Sec. XI [31]). We also reassure that the Rayleigh signals observed in Fig. 3 do not include any other nearby nanotubes with a careful low-magnification TEM examination. DWCNT (12,11)@(17,16) also exhibits a reasonably uniform Rayleigh optical response when tracing the laser beam along its axis (also see Supplemental Material, Sec. VIII [31]), with no sign of the presence of large impurities. Transitions between different subbands (e.g., S_{13}, S_{24}, etc.) from each individual constituent nanotube also cannot explain our experimental observation. These transitions are not allowed when the laser polarization direction is parallel to the nanotube axis as in our experiment [40]. The optical response measured with a cross-polarized laser beam is found negligibly small (Supplemental Material, Sec. XII [31]). Emission from single defects also cannot explain the extra peaks, since if they exist, they would emit light with an energy well below the visible range (the band gap of outer nanotube lies in mid-infrared).

In summary, we show the first experimental observation of a strong-coupling effect in a structure-identified 1D moiré superlattice. Through combining TEM-based chirality assignment and optical susceptibility measurements with Rayleigh scattering spectroscopy, we have successfully observed optical responses from a strong-coupled DWCNT, (12,11)@(17,16). In contrast to DWCNTs in the much more frequently observed weak-coupling regime, such as (15,13)@(21,17) and (23,4)@(22,18), the Rayleigh scattering spectrum of (12,11)@(17,16) cannot be understood based on the simple sum of individual (12,11) and (17,16) nanotubes. Our numerical simulation shows that the moiré superlattice potential leads to a significant alteration of the band structure of (12,11)@(17,16) and the corresponding optical absorption spectrum, which is qualitatively consistent with our experimental observation and interpretation. This is the first definitive experimental observation of a significant moiré superlattice effect on a structure-identified 1D system, which will lead to extended exploration of rich moiré physics in 1D such as strongly correlated physics, moiré excitons, and superconductivity.

We acknowledge Dr. SeokJae Yoo in the Department of Physics, UC Berkeley for the helpful discussion. P. M. acknowledges the support from Science and Technology Commission of Shanghai Municipality Grant No. 19ZR1436400, and NYU-ECNU Institute of Physics at NYU Shanghai. This work was supported by JSPS KAKENHI Grants No. JP17K05496, No. JP16H06331, No. JP16H03825, No. JP16H00963, No. JP15K13283, and No. JP25107002 and JST CREST Grant No. JPMJCR16F3.

*To whom correspondence should be addressed.
sihanzhao88@berkeley.edu
†To whom correspondence should be addressed.
r.kitaura@nagoya-u.jp

[1] C. R. Dean *et al.*, Hofstadter's butterfly and the fractal quantum Hall effect in moiré superlattices, Nature (London) **497**, 598 (2013).
[2] L. A. Ponomarenko *et al.*, Cloning of Dirac fermions in graphene superlattices, Nature (London) **497**, 594 (2013).
[3] B. Hunt *et al.*, Massive Dirac fermions and Hofstadter butterfly in a van der Waals heterostructure, Science **340**, 1427 (2013).
[4] A. K. Geim and I. V. Grigorieva, Van der Waals heterostructures, Nature (London) **499**, 419 (2013).
[5] R. Bistritzer and A. H. MacDonald, Moiré bands in twisted double-layer graphene, Proc. Natl. Acad. Sci. U.S.A. **108**, 12233 (2011).
[6] Y. Cao *et al.*, Correlated insulator behaviour at half-filling in magic-angle graphene superlattices, Nature (London) **556**, 80 (2018).

[7] Y. Cao, V. Fatemi, S. Fang, K. Watanabe, T. Taniguchi, E. Kaxiras, and P. Jarillo-Herrero, Unconventional superconductivity in magic-angle graphene superlattices, Nature (London) **556**, 43 (2018).
[8] H. C. Po, L. Zou, A. Vishwanath, and T. Senthil, Origin of Mott Insulating Behavior and Superconductivity in Twisted Bilayer Graphene, Phys. Rev. X **8**, 031089 (2018).
[9] M. Koshino, N. F. Q. Yuan, T. Koretsune, M. Ochi, K. Kuroki, and L. Fu, Maximally Localized Wannier Orbitals and the Extended Hubbard Model for Twisted Bilayer Graphene, Phys. Rev. X **8**, 031087 (2018).
[10] G. Chen *et al.*, Evidence of a gate-tunable Mott insulator in a trilayer graphene moiré superlattice, Nat. Phys. **15**, 237 (2019).
[11] H. Yu, G. Bin Liu, J. Tang, X. Xu, and W. Yao, Moiré excitons: From programmable quantum emitter arrays to spin-orbit–coupled artificial lattices, Sci. Adv. **3**, e1701696 (2017).
[12] F. Wu, T. Lovorn, and A. H. Macdonald, Topological Exciton Bands in Moiré Heterojunctions, Phys. Rev. Lett. **118**, 1 (2017).
[13] K. Tran *et al.*, Evidence for moiré excitons in van der Waals heterostructures, Nature (London) **567**, 71 (2019).
[14] K. L. Seyler, P. Rivera, H. Yu, N. P. Wilson, E. L. Ray, D. G. Mandrus, J. Yan, W. Yao, and X. Xu, Signatures of moiré-trapped valley excitons in MoSe2/WSe2 heterobilayers, Nature (London) **567**, 66 (2019).
[15] C. Jin *et al.*, Observation of moiré excitons in WSe2/WS2 heterostructure superlattices, Nature (London) **567**, 76 (2019).
[16] E. M. Alexeev *et al.*, Resonantly hybridized excitons in moiré superlattices in van der Waals heterostructures, Nature (London) **567**, 81 (2019).
[17] S. Sanvito, Y. K. Kwon, D. Tománek, and C. J. Lambert, Fractional Quantum Conductance in Carbon Nanotubes, Phys. Rev. Lett. **84**, 1974 (2000).
[18] M. Kociak, K. Suenaga, K. Hirahara, Y. Saito, T. Nakahira, and S. Iijima, Linking Chiral Indices and Transport Properties of Double-Walled Carbon Nanotubes, Phys. Rev. Lett. **89**, 155501 (2002).
[19] Y. Tison, C. E. Giusca, V. Stolojan, Y. Hayashi, and S. R. P. Silva, The inner shell influence on the electronic structure of double-walled carbon nanotubes, Adv. Mater. **20**, 189 (2008).
[20] R. Bonnet, A. Lherbier, C. Barraud, M. Luisa Della Rocca, P. Lafarge, and J.-C. Charlier, Charge transport through one-dimensional Moiré crystals, Sci. Rep. **6**, 19701 (2016).
[21] Y. K. Kwon, S. Saito, and D. Tománek, Effect of intertube coupling on the electronic structure of carbon nanotube ropes, Phys. Rev. B **58**, R13314 (1998).
[22] Ph. Lambin, V. Meunier, and A. Rubio, Electronic structure of polychiral carbon nanotubes, Phys. Rev. B **62**, 5129 (2000).
[23] S. Uryu and T. Ando, Electronic intertube transfer in double-wall carbon nanotubes, Phys. Rev. B **72**, 245403 (2005).
[24] Y. Tomio, H. Suzuura, and T. Ando, Interwall screening and excitons in double-wall carbon nanotubes, Phys. Rev. B **85**, 085411 (2012).
[25] D. Levshov *et al.*, Experimental evidence of a mechanical coupling between layers in an individual double-walled carbon nanotube, Nano Lett. **11**, 4800 (2011).
[26] S. Zhao, T. Kitagawa, Y. Miyauchi, K. Matsuda, H. Shinohara, and R. Kitaura, Rayleigh scattering studies on inter-layer interactions in structure-defined individual double-wall carbon nanotubes, Nano Res. **7**, 1548 (2014).
[27] T. C. Hirschmann, P. T. Araujo, H. Muramatsu, J. F. Rodriguez-Nieva, M. Seifert, K. Nielsch, Y. Ahm Kim, and M. S. Dresselhaus, Role of intertube interactions in double- and triple-walled carbon nanotubes, ACS Nano **8**, 1330 (2014).
[28] K. Liu, C. Jin, X. Hong, J. Kim, A. Zettl, E. Wang, and F. Wang, Van der Waals-coupled electronic states in incommensurate double-walled carbon nanotubes, Nat. Phys. **10**, 737 (2014).
[29] M. Koshino, P. Moon, and Y. W. Son, Incommensurate double-walled carbon nanotubes as one-dimensional moiré crystals, Phys. Rev. B **91**, 035405 (2015).
[30] S. Berciaud, C. Voisin, H. Yan, B. Chandra, R. Caldwell, Y. Shan, L. E. Brus, J. Hone, and T. F. Heinz, Excitons and high-order optical transitions in individual carbon nanotubes: A Rayleigh scattering spectroscopy study, Phys. Rev. B **81**, 041414 (2010).
[31] See Supplemental Material at http://link.aps.org/supplemental/10.1103/PhysRevLett.124.106101 for experimental and theoretical results on the DWCNT structures and spectra, which includes Refs. [29,32–36].
[32] K. Liu *et al.*, An atlas of carbon nanotube optical transitions, Nat. Nanotechnol. **7**, 325 (2012).
[33] S. Choi, J. Deslippe, R. B. Capaz, and S. G. Louie, An explicit formula for optical oscillator strength of excitons in semiconducting single-walled carbon nanotubes: Family behavior, Nano Lett. **13**, 54 (2013).
[34] S. Uryu, Electronic states and quantum transport in double-wall carbon nanotubes, Phys. Rev. B **69**, 075402 (2004).
[35] T. Ando, Theory of electronic states and transport in carbon nanotubes, J. Phys. Soc. Jpn. **74**, 777 (2005).
[36] M. Koshino and N. N. T. Nam, Continuum model for relaxed twisted bilayer graphenes and moiré electron-phonon interaction, arXiv:1909.10786.
[37] Z. Liu and L. C. Qin, A direct method to determine the chiral indices of carbon nanotubes, Chem. Phys. Lett. **408**, 75 (2005).
[38] K. Liu *et al.*, Direct determination of atomic structure of large-indexed carbon nanotubes by electron diffraction: Application to double-walled nanotubes, J. Phys. D **42**, 125412 (2009).
[39] O. N. Torrens, M. Zheng, and J. M. Kikkawa, Direct Experimental Evidence of Exciton-Phonon Bound States in Carbon Nanotubes, Phys. Rev. Lett. **101**, 157401 (2008).
[40] S. Uryu and T. Ando, Exciton absorption of perpendicularly polarized light in carbon nanotubes, Phys. Rev. B **74**, 155411 (2006).